1
An Introduction to Graphene

Konstantinos Spyrou and Petra Rudolf

1.1
Brief History of Graphite

Carbon takes its name from the latin word *carbo* meaning charcoal. This element is unique in that its unique electronic structure allows for hybridization to build up sp^3, sp^2, and sp networks and, hence, to form more known stable allotropes than any other element. The most common allotropic form of carbon is *graphite* which is an abundant natural mineral and together with diamond has been known since antiquity. Graphite consists of sp^2 hybridized carbon atomic layers which are stacked together by weak van der Waals forces. The single layers of carbon atoms tightly packed into a two-dimensional (2D) honeycomb crystal lattice is called *graphene*. This name was introduced by Boehm, Setton, and Stumpp in 1994 [1]. Graphite exhibits a remarkable anisotropic behavior with respect to thermal and electrical conductivity. It is highly conductive in the direction parallel to the graphene layers because of the in-plane metallic character, whereas it exhibits poor conductivity in the direction perpendicular to the layers because of the weak van der Waals interactions between them [2]. The carbon atoms in the graphene layer form three σ bonds with neighboring carbon atoms by overlapping of sp^2 orbitals while the remaining p_z orbitals overlap to form a band of filled π orbitals – the valence band – and a band of empty π^* orbitals – the conduction band – which are responsible for the high *in-plane* conductivity.

The interplanar spacing of graphite amounts to 0.34 nm and is not big enough to host organic molecules/ions or other inorganic species. However several intercalation strategies have been applied to enlarge the interlayer galleries of graphite from 0.34 nm to higher values, which can reach more than 1 nm in some cases, depending on the size of the guest species. Since the first intercalation of potassium in graphite, a plethora of chemical species have been tested to construct what are known as graphite intercalation compounds (GICs). The inserted species are stabilized between the graphene layers through ionic or polar interactions without influencing the graphene structure. Such compounds can be formed not only with lithium, potassium, sodium, and other alkali metals, but also with anions such as nitrate, bisulfate, or halogens.

Functionalization of Graphene, First Edition. Edited by Vasilios Georgakilas.

In other cases the insertion of guest molecules may occur through covalent bonding via chemical grafting reactions within the interlayer space of graphite; this results in structural modifications of the graphene planes because the hybridization of the reacting carbon atoms changes from sp^2 to sp^3. A characteristic example is the insertion of strong acids and oxidizing reagents that creates oxygen functional groups on the surfaces and at the edges of the graphene layers giving rise to graphite oxide. Schafheutl [3] first (1840) and Brodie [4] 19 years later (1859) were the pioneers in the production of graphite oxide. The former prepared graphite oxide with a mixture of sulfuric and nitric acid, while the latter treated natural graphite with potassium chlorate and fuming nitric acid. Staudenmaier [5] proposed a variation of the Brodie method where graphite is oxidized by addition of concentrated sulfuric and nitric acid with potassium chlorate. A century later (1958) Hummers and Offeman [6] reported the oxidation of graphite and the production of graphite oxide on immersing natural graphite in a mixture of H_2SO_4, $NaNO_3$, and $KMnO_4$ as a result of the reaction of the anions intercalated between the graphitic layers with carbon atoms, which breaks the aromatic character. The strong oxidative action of these species leads to the formation of anionic groups on graphitic layers, mostly hydroxylates, carboxylates, and epoxy groups. The out of planar C–O covalent bonds increase the distance between the graphene layers from 0.35 nm in graphite to about 0.68 nm in graphite oxide [7]. This increased spacing and the anionic or polar character of the oxygen groups formed impart to graphene oxide (GO) a strongly hydrophilic behavior, which allows water molecules to penetrate between the graphene layers and thereby increase the interlayer distance even further. Thus graphite oxide becomes highly dispersible in water. The formation of sp^3 carbon atoms during oxidation disrupts the delocalized π system and consequently electrical conductivity in graphite oxide deteriorates reaching between 10^3 and $10^7\ \Omega$ cm depending on the amount of oxygen [2, 8].

1.2 Graphene and Graphene Oxide

For several decades the isolation of graphene monolayer seemed to be impossible on the basis of, among other things, theoretical studies on the thermodynamic stability of two-dimensional crystals [9]. An important step in this direction was made by a research group in Manchester guided by Geim and Novoselov in 2004 [10] who reported a method for the creation of single layer graphene on a silicon oxide substrate by peeling the graphite by micromechanical cleavage (scotch tape method). Graphene exhibited outstanding structural [11], electrical [12], and mechanical properties [13] and 6 years later Novoselov and Geim were honored with the Nobel Prize in Physics *"for groundbreaking experiments regarding the two-dimensional material graphene."* During this time a number of methods for the production of graphene monolayers have been developed. These methods can be divided into different categories depending on the chemical or physical process

employed to obtain the single layer graphene. The next three sections describe the three types of chemical methods.

1.2.1
Preparation of Graphene from Graphene Oxide

Although the report on single sheets of GO [14, 15] obtained by procedures established by Staudenmaier and Hummers and Offeman [4–6] had been published, the scientific community largely continued to consider graphite oxide a layered graphitic material. It was not until after the isolation of pristine graphene by micromechanical cleavage that the question was reexamined and it was ascertained that the method developed by Hummers and Offeman produces exfoliated oxidized single graphene layers by the dispersion of graphite oxide in water. These chemically prepared monolayers of GO can be considered the precursors for the production of graphene by the removal of the oxygen groups. The precise structure of GO depends on the oxidation process and is still a subject of debate. The most accepted models are the Lerf–Klinowski and the Dékány models [16, 17]. Recently Ajayan *et al*. confirmed that for GO prepared with the protocol that resulted in the Lerf–Klinowski model, ring lactols are present at the edges of the GO sheets (Figure 1.1) [18].

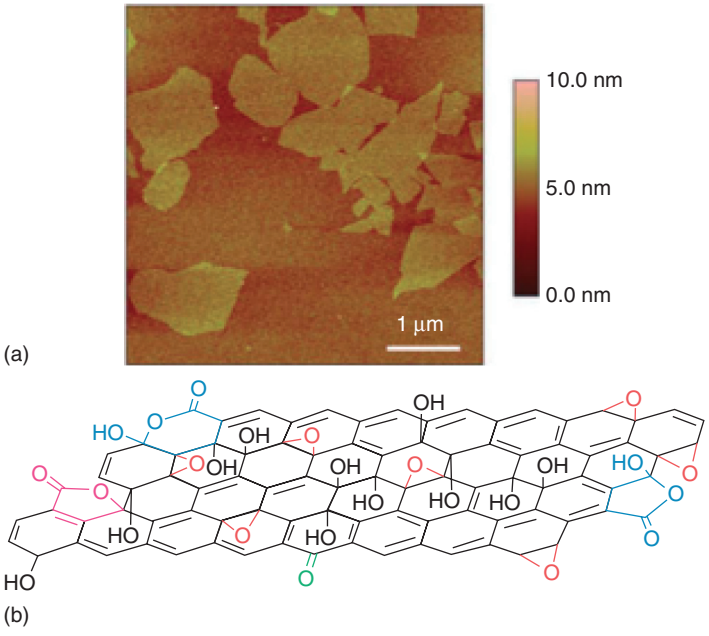

Figure 1.1 Atomic force microscopy (AFM) image and structural model of graphene oxide (GO) sheets. (a) An AFM image of GO sheets on a silicon substrate. (b) A structural model of GO introduced by Ajayan *et al*. (Reproduced with permission from [18].)

Table 1.1 Summary of reduction agents for chemical reduction of graphene oxide [22].

Reduction agent	Temperature (°C) during reduction	Reduction time (*h*)	Electrical conductivity ($S\,m^{-1}$) after reduction	References
Hydrazine	100	24	$\sim 2 \times 10^2$	[20]
Hydroquinone	25	20	—	[23]
Alkali	50–90	A few minutes	—	[24]
Sodium borohydride	25	2	$\sim 4.5 \times 10^1$	[25]
Ascorbic acid (vitamin C)	95	24	$\sim 7.7 \times 10^3$	[26]
Hydroiodic acid	100	1	$\sim 3 \times 10^4$	[27]
Hydroiodic acid (with acetic acid)	40	40	$\sim 3.0 \times 10^4$	[28]
Sulfur-containing compounds[a]	95	3	—	[29]
Pyrogallol	95	1	$\sim 4.9 \times 10^2$	[26]
Benzylamine	90	1.5	—	[30]
Hydroxyl amine	90	1	$\sim 1.1 \times 10^2$	[31]
Aluminum powder (with hydrochloric acid)	25	0.5	$\sim 2.1 \times 10^3$	[32]
Iron powder (with hydrochloric acid)	25	6	$\sim 2.3 \times 10^3$	[33]
Amino acid (L-cysteine)	25	12–72	—	[34]
Sodium hydrosulfite	60	0.25	$\sim 1.4 \times 10^3$	[35]
Alcohols	100	24	$\sim 2.2 \times 10^3$	[23]
Dimethylformamide	153	1	$\sim 1.4 \times 10^3$	[36]

[a] Sulfur-containing compounds include $NaHSO_3$, Na_2S, $Na_2S_2O_3$, $SOCl_2$, and SO_2.

The first dispersion of single graphene layers was presented in 2006 by Ruoff's group, which used hydrazine hydrate for the reduction of GO prepared by Hummers method [19, 20]. Although several reductive procedures have been applied by several research groups (see Table 1.1 and references therein) in the following years, none achieved full reduction of the GO monolayers into graphene. This agrees with the theoretical finding that a reduction of GO from 75% to 6.25% (C:O ratio 16 : 1) coverage is relatively easy but further reduction seems to be rather difficult [21]. For this reason the final isolated carbon monolayers derived from the reduction of GO are usually called partially reduced graphene oxide (*r*GO) or chemically converted graphene (CCG). The results of the various reductive procedures that have been developed are summarized in the following table.

Reduction of GO can be also be achieved via thermal annealing at temperatures >1000 °C [36], photochemical reduction [37], and electrochemical reduction [38, 39]. One of the biggest disadvantages of GO is the very low electrical conductivity. According to theory, GO becomes conducting when the functional groups

reach 25% [21]. After the removal of the oxygen groups, *r*GO can be further graphitized by annealing at elevated temperatures. In this process defects that remain after reduction are rearranged and the aromatic character of the monolayers increases. However, the presence of oxygen groups on the graphene surface is not always undesirable. In fact, by exploiting the well-established carbon chemistry the oxygen functional groups can be used for further functionalization of the layers for applications in catalysis, gas sensors, energy storage, and environmental remediation.

1.2.2 Isolation of Pristine Graphene Monolayers

Exfoliation of graphite into single graphene layers can also be achieved by ultrasonication in organic solvents. Acoustic cavitation provides unusual chemical conditions because extremely high temperatures and pressures are reached for short times in the liquid [40]. If the free energy of mixing is negative and the solvent is able to stabilize colloidal graphene because its surface energy matches that of graphene, the graphitic basal structure is broken and small graphite fragments intercalated by solvent molecules are produced [41, 42]. Dimethylformamide (DMF) [43], *N*-methyl pyrrolidone (NMP) [41], pyridine and other perfluorinated solvents [44], and *o*-dichlorobenzene [45] were the first solvents successfully used for this purpose (Figure 1.2).

Sonication methods usually provide a mixture of several derivatives where single graphene represents a percentage of 1–15% and the rest consists of few-layer graphene nanosheets, where the number of layers range from 2 to 10 [41, 44]. The final percentage of single graphene layers can be increased by selective centrifugation. The advantage in these methods is that the graphitic character of the exfoliated layers is less affected than in oxidation. However the implosion of cavitation bubbles causes violent collisions between particles at very high speed

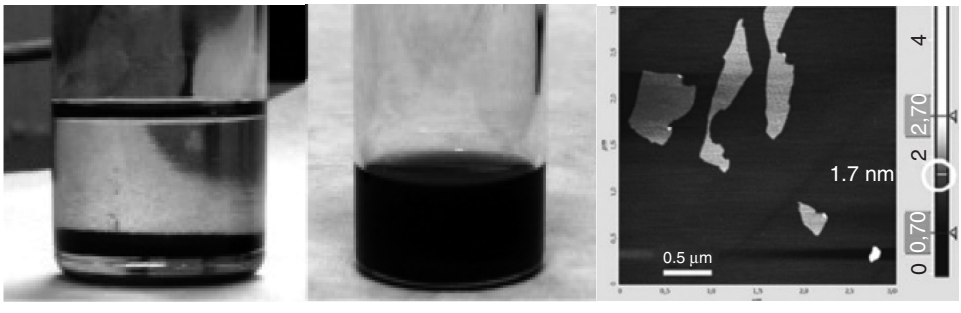

(a) (b) (c)

Figure 1.2 (a) Graphite precipitation in benzene after sonication; and (b) partial exfoliation of graphite in pyridine by sonication affords a dark colloidal dispersion with concentration 0.3 mg ml^{-1}. (c) AFM image of several pyridine-etched single graphenes layers. (Reproduced with permission from [44].)

that, in air-saturated sonicated solutions, dissociate the solvent and form peroxyl radicals [46]. The radical reactions are usually destructive and very effective in breaking C–C bonds [47]. Consequently prolonged sonication treatments result in a reduction of the sheet size and a higher number of defects [48] mostly consisting in oxidized carbon atoms at graphene edges in the form of epoxy, carbonyl, and carboxyl groups [49]. Such damage during exfoliation of graphite in DMF can be considerably reduced by the addition of *N*-2-mercapto-propionyl glycine (tiopronin), a molecule that inhibits reactions promoted by oxygen, peroxides, and radicals [50]. An alternative route to sonication, which also has the advantage of mitigating the development of defects, is the method developed by Ester Vazquez *et al*. who have used mechanochemical activation by ball-milling to exfoliate graphite through interactions with melamine (2,4,6-triamine-1,3,5-triazine) under solid conditions [51].

1.2.3
Large Scale Production of GO by Langmuir-Blodgett Methods

A simple protocol to deposit large GO flakes (5–20 μm) makes use of the Langmuir–Blodgett technique (LB) [52, 53] where a highly diluted and well dispersed water solution of GO is employed as a subphase for the LB deposition.

By applying external pressure through the movable barriers of a LB trough the packing of the GO layers floating at the air–water interface can be modified. Different from molecular and hard colloidal particle monolayers, the GO single layer flakes tend to fold and wrinkle to resist collapsing into multilayers. The first report of large-flake production of GO by using the LB method and controllable deposition was presented by Cote *et al*. [52]. As illustrated in Figure 1.3 by controlling the surface pressure, a high coverage of the GO sheets can be achieved and the method is suitable for large scale production. The injection of a long-chain molecule (e.g., octadecylamine) at the air–water interface causes the GO sheets to bind covalently and results in the formation of surfactant-GO layers [53]. This hybrid Langmuir film can be transferred to an arbitrary support (higher hydrophobicity of the substrate increases the transfer ratio and the quality of the deposited layer) by horizontally lowering the desired substrate to contact the surfactant-GO-water interface – this way of transferring is known as the *Langmuir–Schaefer method*.

1.2.4
Other Methods of Graphene Production

Alternative ways for the production of single graphene layers via physical and physicochemical routes are less relevant for the present monograph and are therefore only briefly mentioned in this section for completeness. Single graphene layers can be produced with very good results by thermal annealing of silicon carbide (SiC) [54] and chemical vapor deposition (CVD) [55–61]. Although several transition metals have been used as catalysts in graphene production, nickel

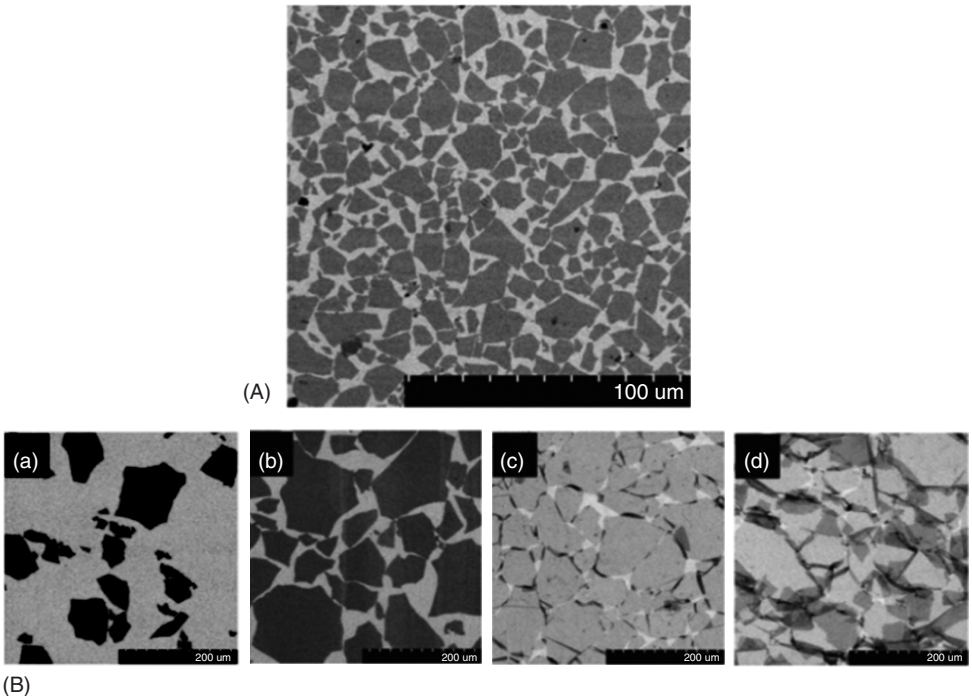

Figure 1.3 (A) SEM (scanning electron microscope) images of highly covered graphene oxide monolayers, scale bar of 100 μm. Langmuir–Blodgett assembly of graphene oxide layers. (B) (a–d) SEM images of graphene oxide layers on a silicon wafer for different surfaces pressures. The packing density gradually increased by controlling the water interface pressure: (a) dilute monolayer of isolated flat sheets, (b) monolayer of close-packed GO, (c) over-packed monolayer with sheets folded at interconnected edges, and (d) over packed monolayer with folded and partially overlap sheets. (Reproduced with permission from [52].)

and copper are the most promising, taking into account their low cost also. On the other hand the thermal annealing of SiC at high temperatures that range between 1000 and 1600 °C results in the sublimation of silicon atoms and the graphitization of the remaining carbon atoms. Another interesting method for the preparation of graphene sheets with predetermined size, also called *graphene nanoribbons*, is the chemical unzipping of multiwalled carbon nanotubes [62]. More precisely, the carbon nanotubes are cut along their axis by plasma etching or strong oxidation. A scheme that presents several procedures for the preparation of graphene nanoribbons as well as an atomic force microscopy (AFM) image of these graphene structures are shown in Figure 1.4. Graphene nanoribbons have the length of the nanotube and their width is equal to the circumference of the nanotube. Their electronic properties are largely determined by the edge structure (armchair or zigzag) and, for certain edge structures, exhibit an energy gap which increases with decreasing width of the nanoribbon [63].

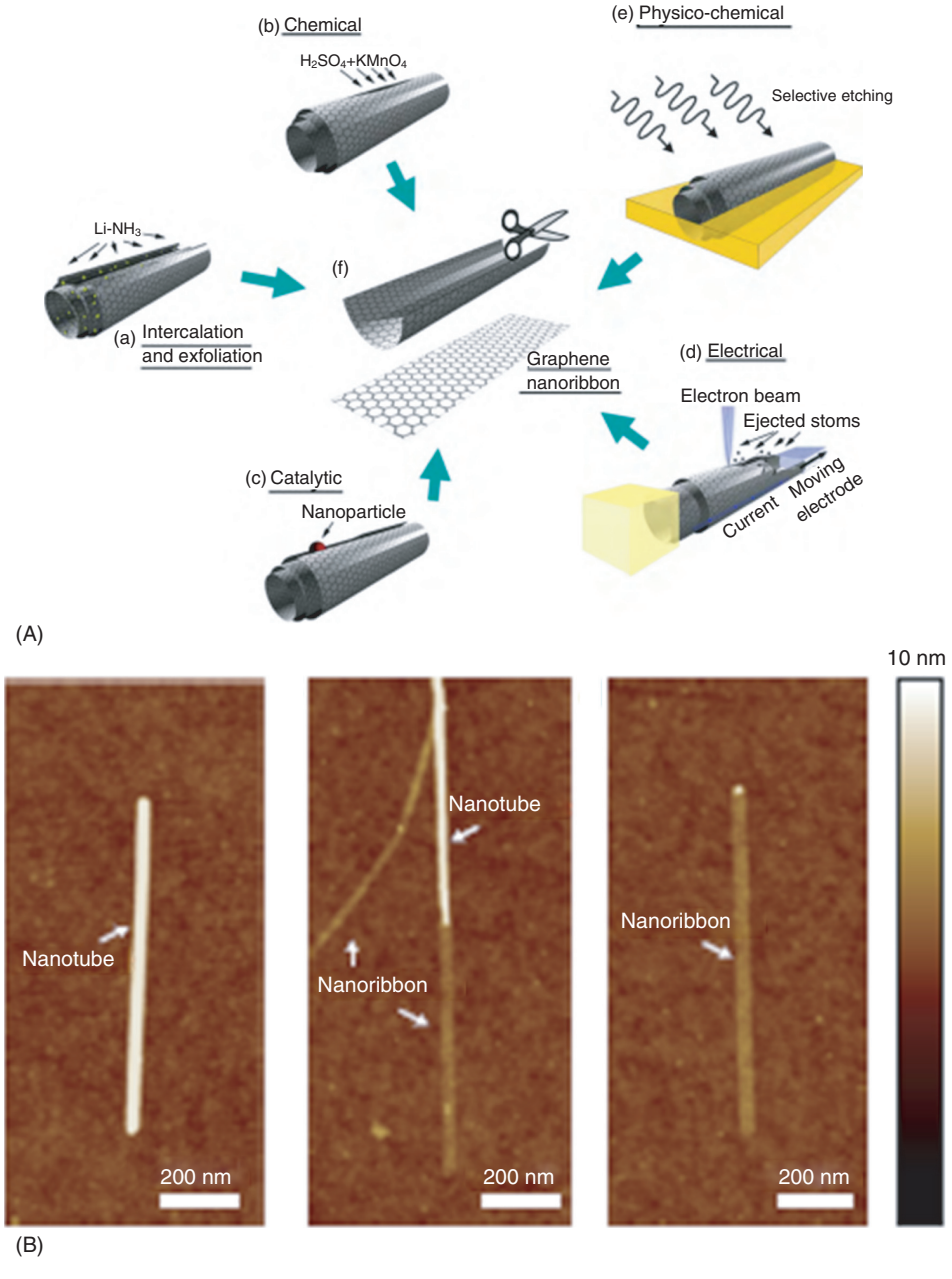

Figure 1.4 (A) Schematic representation of the several ways to unzip carbon nanotubes and produce graphene nanoribbons. (Reproduced with permission from [62].) (B) Characteristic AFM images of graphene nanoribbons by unzipping carbon nanotubes. (Reproduced with permission from [64].)

1.3 Characterization of Graphene

The isolation of single graphene sheets offers opportunities for its investigation by various spectroscopic and microscopic techniques; samples can be either in the form of dispersion or graphene sheets deposited on the proper substrates. In this section the most commonly used characterization tools are introduced. As for most nanomaterials electronic microscopies and AFM are powerful tools for the characterization of graphene and graphene derivatives. Raman spectroscopy and spectromicroscopy can distinguish single layer graphene from double layer and few-layer graphene and give clear indications on the number of defects present in the material. Thermogravimetric analysis (TGA) diagrams are useful to trace changes in the structure of graphitic materials before and after functionalization of graphene sheets. Optical microscopy can visualize a single graphene layer that is placed on the right substrate. X-ray diffraction (XRD) informs on the success of exfoliation or intercalation of graphite and is particularly useful to demonstrate functionalization.

1.3.1 Microscopic Observation

The characterization of a graphene material by AFM is often performed by drop casting or spin coating a highly diluted graphene dispersion on a silicon wafer since such deposits are flat enough to allow for recording of height differences on the monoatomic level. Figure 1.5A shows representative AFM images of single graphene sheets. One can clearly observe the height differences between the flat and folded part of the graphene layer. The average height of annealed single layer graphene flakes is typically in the range of 0.8–1.2 nm when decorated with oxygen- and hydro-containing groups [65]. After graphitization treatments at high temperature, the average height of the flakes drops to 0.3–0.5 nm [55], showing the ''fingerprint'' of a single atomic sheet as similar to the mechanically exfoliated flakes [66].

Typical TEM (transmission electron microscope) images of single layer graphene are presented in Figure 1.5B-a,b; the film is almost transparent. When recorded with aberration-corrected instruments defect structures at grain boundaries can be imaged with atomic resolution as shown in Figure 1.5B-c. The atomic structure of graphene sheets is visualized by exit wave reconstruction, which is an advanced TEM technique in which 10–30 HR-TEM images are acquired at different defocus values and combined into the complex wave of electrons at the exit plane of the sample. An example of a phase image of such an exit wave of electrons leaving a graphene sheet is presented in Figure 1.5B-d [50]. In contrast to single high resolution TEM images, phase images allow for a quantitative interpretation of the contrast and permit to distinguish single and double graphene layers [69]. The inset of Figure 1.5B-d shows a defect-free graphene lattice, in which the positions of the

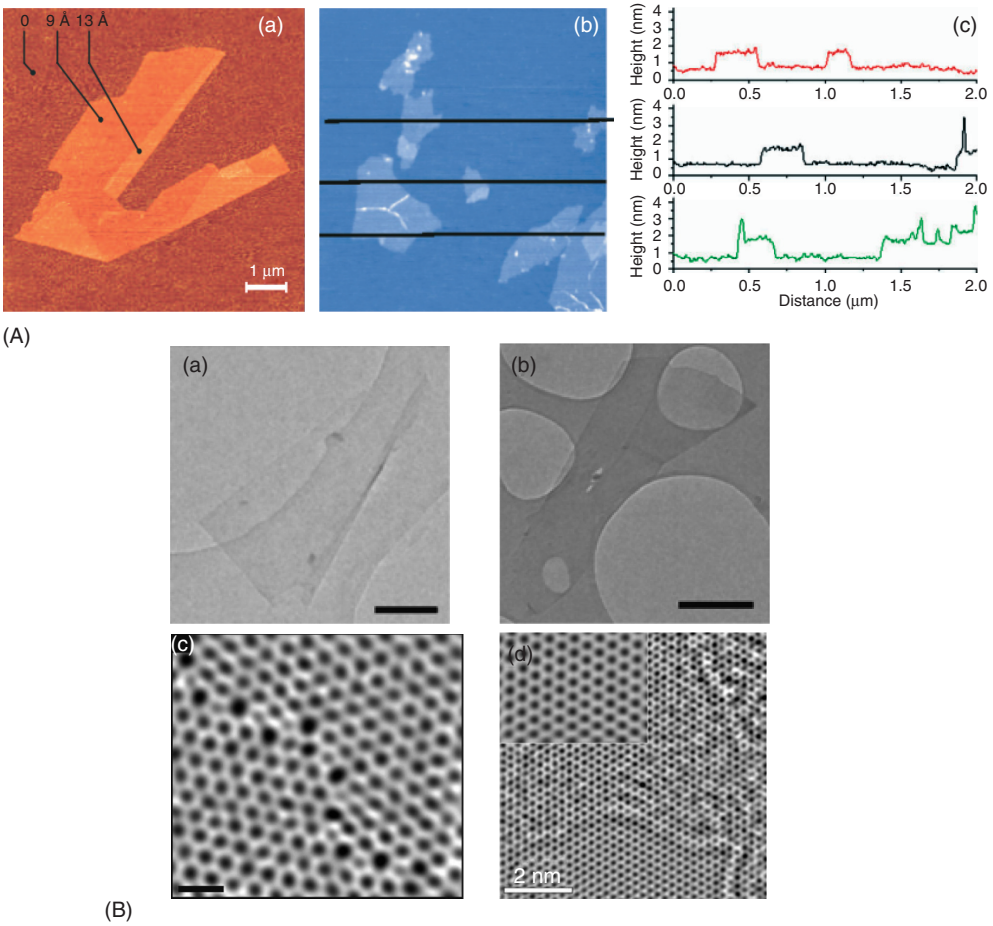

Figure 1.5 (A) (a) AFM image of pristine single graphene sheet. The height which corresponds to the thickness of a single layer is 0.9 nm while a folded sheet is measured at height of 1.3 nm. (Reproduced with permission from [67].) (b) AFM image and height profile of a single GO layer. (Reproduced with permission from [20].) (c) height profile collected along the lines marked in black on the AFM micrograph. (B) TEM images of (a,b) pristine single graphene sheets. (Reproduced with permission from [41].) (c) Aberration-corrected TEM image: grain boundary in a single graphene sheet. (Reproduced with permission from [68].) (d) HR-TEM of a graphene monolayer produced by exfoliation of graphite in the presence of tiopronin as radical trap. (Reproduced with permission from [50].)

individual carbon atoms can be distinguished. This image clearly indicates a single graphene sheet, as the AB stacking of a double sheet would lead to the presence of additional atoms in the center of the hexagons. The overview image shown in Figure 1.5B-d also indicates that adsorbents are likely to be present at the surface of the graphene layer giving rise to the ripple-like contrast present in this image.

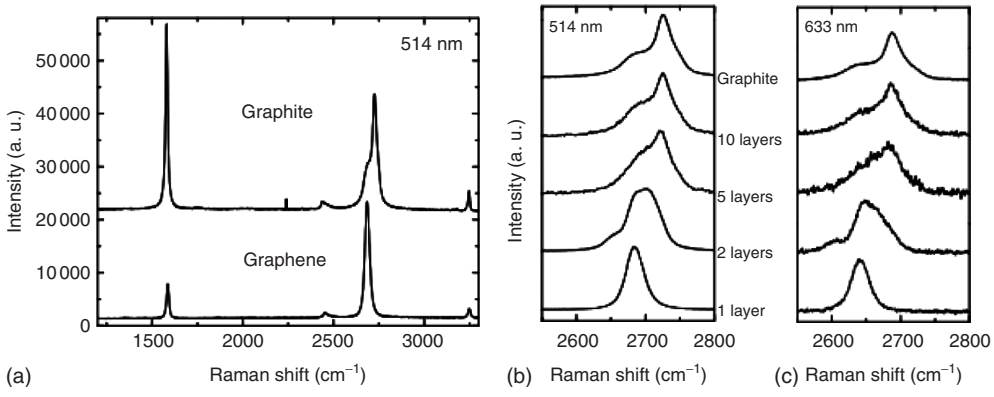

Figure 1.6 (a–c) The Raman spectra of pristine graphene in comparison with that of graphite and the G′ band of several multilayered graphene nanosheets. (Reproduced with permission from [70].)

1.3.2 Raman Spectroscopy

Raman spectroscopy is a widely used tool for the characterization of carbon materials; it is particularly informative on the structure of graphene nanosheets regarding the number of graphene layers, as well as the existence of defects and the extent of functionalization. The pioneering study of the Raman spectrum of pristine single graphene was by Ferrari *et al*. [70] which, as shown in Figure 1.6, explained how for few-layer graphene consisting of – one to five layers, the precise number of layers can be extracted from the spectrum. The Raman spectrum of a pristine single graphene layer has two characteristic features at 1580 cm^{-1}, and at 2700 cm^{-1} called the *G band* and the *G′ band*, respectively [71]. The G band is a result of the doubly degenerate zone center E_{2g} mode [72]. The G band also bears testimony to the number of layers. As the layer thickness increases, the band position shifts to lower wavenumbers conforming to the calculated positions for these band locations. The position of the G band is also sensitive to doping and strain leads to splitting of this band [73]. The G′ band is the second order of zone boundary phonons and very often referred to as *2D band*. The first order of the zone boundary phonons is only observed as a peak around 1350 cm^{-1}, called *D band*, when graphene has a sufficient number of defect sites. In the case of a pristine graphene monolayer produced by micromechanical cleavage such a band is not detected because of the lack of defects [73].

As seen in Figure 1.6c, the G′ peak changes with the number of layers: The G′ peak of a single layer of graphene is a sharp symmetrical peak below 2700 cm^{-1}. For bilayer graphene this peak is shifted to slightly higher wave numbers and becomes broader with a shoulder toward lower wavenumbers. As the number of the layers increases the peak shifts to higher wave numbers and finally in a five layer nanosheet it appears as a broad double peak where the two components have

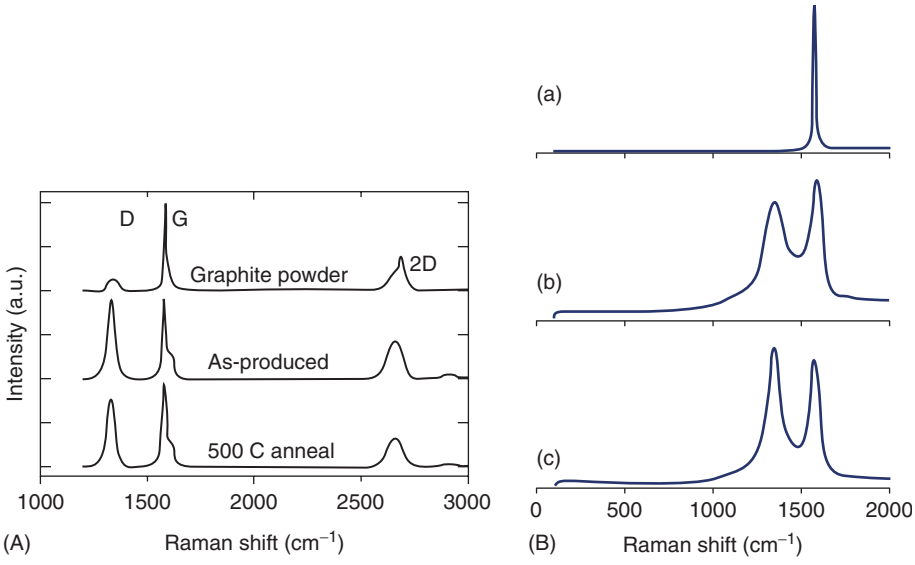

Figure 1.7 (A) Raman spectrum of graphene as produced and after annealing at 500 °C in comparison with that of the starting graphite. (Reproduced with permission from [74].) (B) The Raman spectra of graphite (a), GO (b), and the reduced GO (c). (Reproduced with permission from [20].)

a 1/2 ratio (see Figure 1.6c). For a nanosheet with more than five layers the G′ band is similar to that of a sample with five layers.

Raman spectra without D band are rarely observed for large pristine single graphene sheets prepared by micromechanical cleaving without defects. In most cases pristine graphene sheets have a sufficient number of defects to result in some D band intensity. The height of the D band directly depends on the number of the sp^3 carbon atoms of graphene surface and thus, on the number of defects of the graphene nanosheets. As regards the quality of graphene, D band is an indication for the aromatic character and the ''quality'' of the graphene nanosheet and is related to the production method and the starting material. As an example, Figure 1.7A reports spectra relative to graphene sheets produced by the exfoliation of graphite in water and stabilized with a surfactant which show an intense D band that remains even after annealing at 500 °C [74]. A similarly intense D band is discerned in the Raman spectra of GO sheets. Here the D band is a common characteristic of the Raman spectra since the existence of sp^3 carbon atoms in the graphitic surface goes along with the formation of oxygen groups (see Figure 1.7B) [20].

1.3.3
Thermogravimetric Analysis

Articles related to the characterization of graphene nanosheets and its derivatives typically include TGA since the structural changes of graphitic materials before

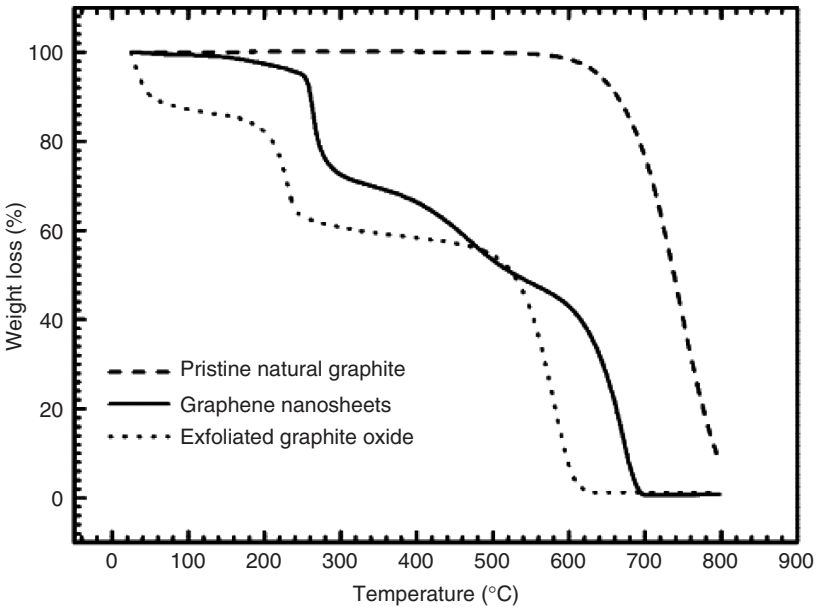

Figure 1.8 TGA curves of natural graphite, *r*GO (graphene nanosheets in the diagram) and exfoliated GO. (Reproduced with permission from [75].)

and after procedures such as the oxidation and exfoliation of graphite or the functionalization of graphene sheets give rise to marked differences in the mass loss as a function of increasing temperature (with constant heating rate). As an example, Figure 1.8 reports the TGA data for Graphite, GO, and *r*GO as presented by Wang *et al*. [75]. The combustion of graphite starts at 650 °C when the sample is heated in air, while GO loses 20% of its weight at 200 °C and is finally decomposed at 550 °C. The first weight loss of GO is attributed to the removal of the oxygen groups while the lower combustion temperature of GO in comparison with graphite demonstrates the lower thermal stability of GO because of the presence of defects created after elimination of oxygen functional moieties. An intermediate thermal behavior is recorded in *r*GO which mirrors the lower number of oxygen groups in this material. For both GO and *r*GO the lower combustion temperature is also influenced by the exfoliation which makes the sheets more easily accessible to air than when they are tightly packed in graphite.

1.3.4
Optical Properties of Graphene

Almost everyone has seen graphene nanosheets deposited on solid substrates. In fact the gray trace left by the movement of a pencil on a white paper is nothing else but overlaid graphene nanosheets. Likewise, if pristine graphene nanosheets are dispersed in organic solvents the liquid shows a gray color and becomes darker

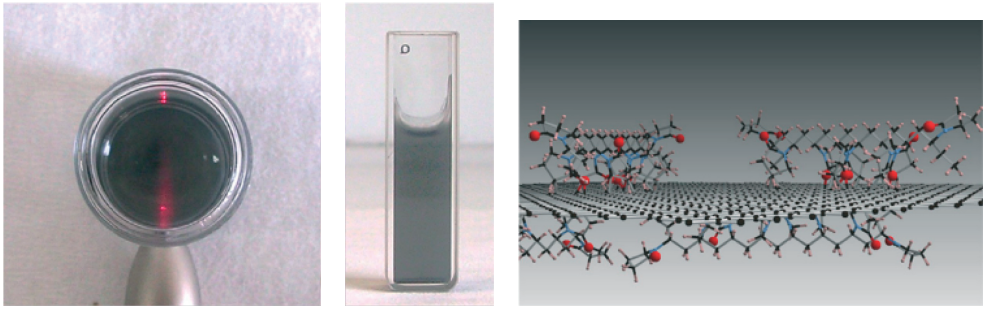

Figure 1.9 (a) A laser beam passing through a dispersion of graphene in water. It is visible due to the Tyndall scattering effect; (b) the optical transparency of a dispersion of graphene in water (0.1 mg ml^{-1}); and (c) schematic model of poly-vinyl pyrrolidone-coated graphene. (Reproduced with permission from [76].)

as the amount of graphene increases. A simple way to identify the presence of nanoparticles in dispersion is based on the Tyndall effect as illustrated in Figure1.9. A laser beam becomes visible passing through the liquid because of the scattering of the light by the dispersed nanoparticles [76].

Graphene as an extended aromatic system has sufficient light absorption; even a single sheet of graphene is visible through an optical microscope if deposited on 300 nm of silicon oxide on top of silicon as a result of an interference effect [10]. After this work several other groups visualized graphene on several other substrates [43, 77, 78]. As shown in Figure 1.10 [79], graphene's optical absorbance of white light has been measured to amount to 2.3%, which means that a bilayer absorbs

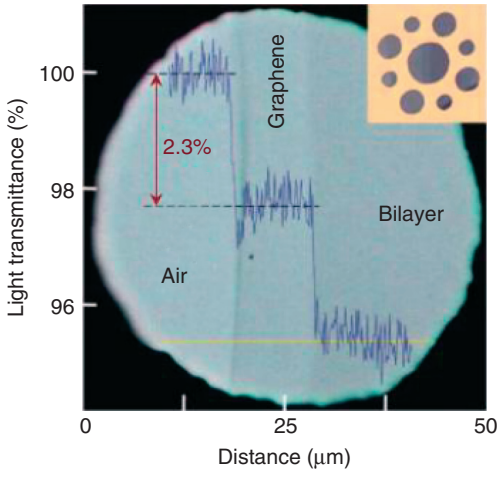

Figure 1.10 A single and a bilayer graphene on a porous membrane. (Reproduced with permission from [80].)

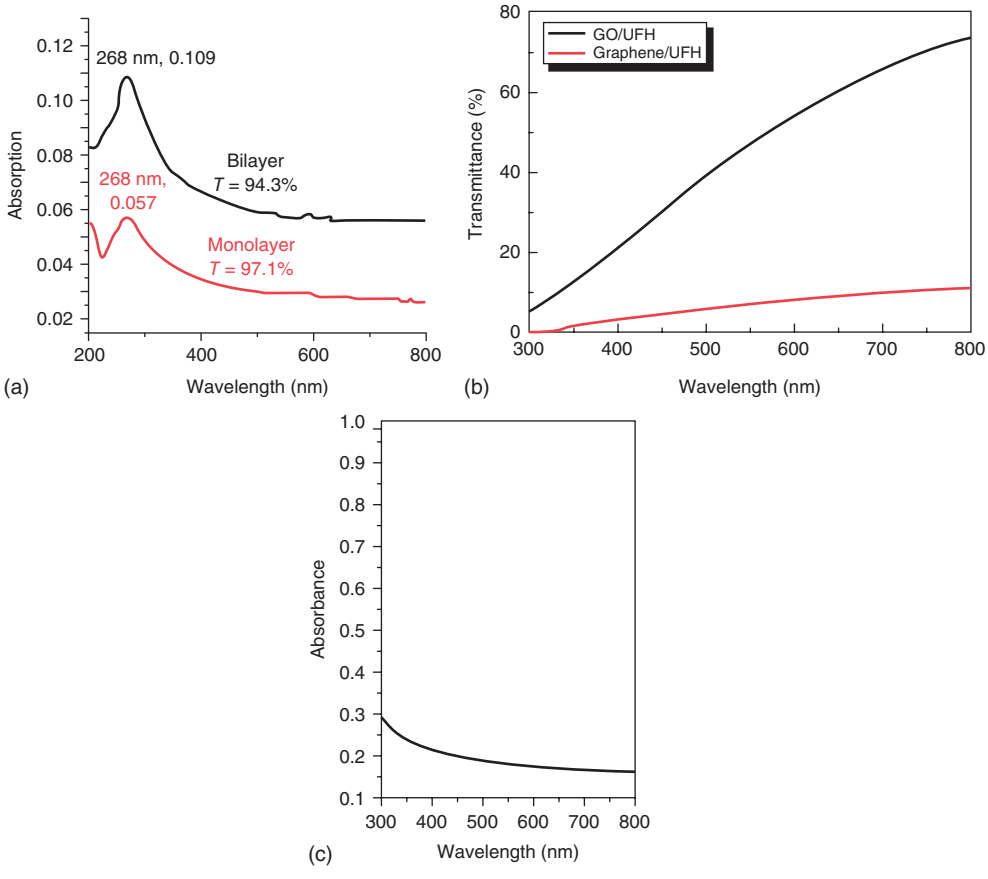

Figure 1.11 (a) The UV–vis absorption spectra of monolayer graphene and bilayer graphene; peaks are labeled with the wavelength of maximum absorption and the value of maximum absorption. The UV transmittance (T, %) is measured at 550 nm. (Reproduced with permission from [81].) (b) UV–vis spectra of GO and graphene in water solution functionalized both with heparin (unfractioned heparin). (Reproduced with permission from [82].) (c): UV–vis spectrum of graphene nanosheets in DMF. (Reproduced with permission from [44].)

4.6% and a five-layer-thick flake near 11.5% [80]. The maximum of the absorption is at 268 nm (Figure 1.11a) [81]. UV–Vis spectrum of graphene/unfractioned heparin production after reduction exhibits remarkable lower transmittance compared to the initial graphite oxide/unfractioned heparin solution (Figure 1.11b). The UV–vis spectrum of graphene flakes dispersed in DMF looks very similar with a continuously rising curve from 700 to 300 nm (Figure 1.11c) [44].

Solid GO has a brownish color and dispersions of GO nanosheets also have a brownish tint. The color becomes darker and grayer as GO is reduced to *r*GO. Because of the different electronic structure, insulated GO has a much

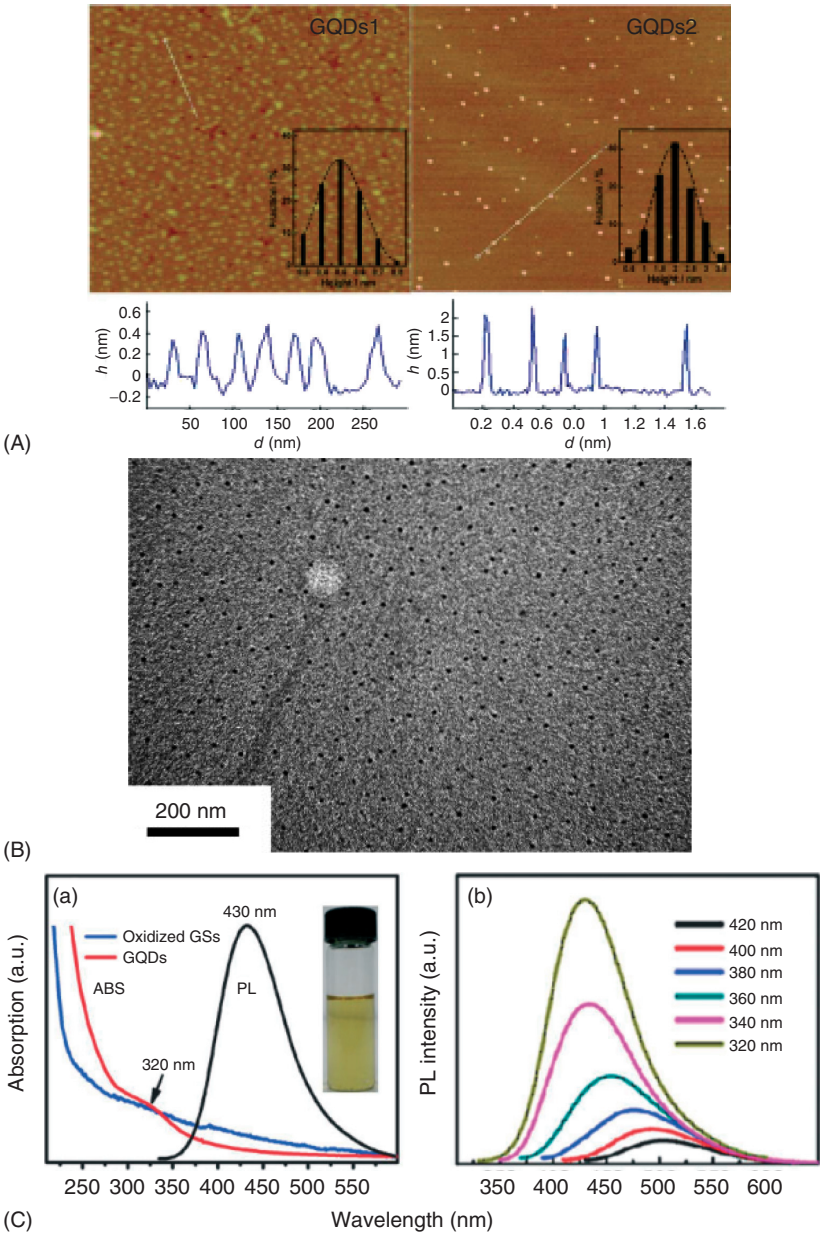

Figure 1.12 (A) and (B) AFM and TEM image of GQDs. (Reproduced with permission from [83, 84].) (C) (a) UV–vis absorption (red line) and photolithography (PL) (at 320 nm excitation) spectra of GQDs dispersed in water; UV–vis absorption (blue line) spectrum of oxidized graphene. Inset: image of GQD aqueous solution. (b) PL spectra of the GQDs at different excitation wavelengths. (Reproduced with permission from [84].)

higher transmittance in comparison to pristine graphene or *r*GO as illustrated in Figure 1.13, upper right panel [82].

The electronic properties of graphene can also be changed by reducing the dimensions of the graphene layers. As illustrated in Figure 1.12, graphene quantum dots (GQDs) consisting of one or few graphene layers with size less than 100 nm show new optoelectronic properties, because of the quantum confinement and the effect of the large percentage of edge atoms. GQDs have a band gap and exhibit a strong photoluminesence, which can be tuned by controlling their size and other morphological factors (Figure 1.12C) [83–88]. Finally the optical transitions in graphene can also be changed by applying a gate voltage in a field-emitting transistor configuration [89]. This is also the way to tune the band gap in bilayer graphene [90].

1.3.5
X-Ray Diffraction Pattern

The different steps for the isolation of graphene from graphite are suitably monitored by collecting XRD patterns of the starting material, intermediates, and the final product. As shown in Figure 1.13, graphite exhibits a basal reflection (002) peak at $2\theta = 26.6°$ which corresponds to a d spacing of 0.335 nm and represents the interlayer distance.

After the oxidation of graphite and before exfoliation the graphite oxide intermediate basal (002) reflection peak is shifted to 11.2° which corresponds to a d spacing of 0.79 nm. This increase in the interlayer space is attributed to the intercalation of

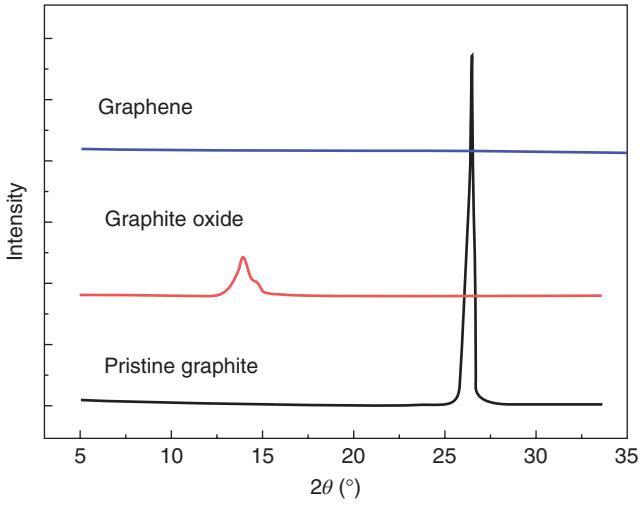

Figure 1.13 X-ray diffraction patterns of pristine graphite, graphite oxide, and graphene. (Reproduced with permission from [91].)

water molecules between the oxidized graphene layers. The width of the strongest diffraction peak can also be used to verify the degree of exfoliation as it is linked to the coherently diffracting domain size via the Debye–Scherrer equation. When graphite oxide is completely exfoliated this diffraction peak disappears [91].

References

1. Boehm, H.P., Setton, R., and Stumpp, E. (1994) *Pure Appl. Chem.*, **66**, 1893.
2. Chung, D.D.L. (2002) *J. Mater. Sci.*, **37**, 1475.
3. Schafheutl, C. (1840) *Philos. Mag.*, **16**, 570.
4. Brodie, B.C. (1859) *Philos. Trans. R. Soc. London*, **149**, 249.
5. Staudenmaier, L. (1898) *Ber. Dtsch. Chem. Ges.*, **31**, 1481.
6. Hummers, W.S. and Offeman, R.E. (1958) *J. Am. Chem. Soc.*, **80**, 1339.
7. Bourlinos, A.B., Gournis, D., Petridis, D., Szabo, T., Szeri, A., and Dekany, I. (2003) *Langmuir*, **19**, 6050.
8. Allen, M.J., Tung, V.C., and Kaner, R.B. (2010) *Chem. Rev.*, **110**, 132.
9. Prezhdo, O.V. (2011) *Surf. Sci.*, **605**, 1607.
10. Novoselov, K.S., Geim, A.K., Morozov, S.V., Jiang, D., Zhang, Y., Dubonos, S.V., Grigorieva, I.V., and Firsov, A.A. (2004) *Science*, **306**, 666.
11. Meyer, J.C., Geim, A.K., Katsnelson, M.I., Novoselov, K.S., Booth, T.J., and Roth, S. (2007) *Nature*, **446**, 60–63.
12. Castro, N., Guinea, F., Peres, N.M.R., Novoselov, K.S., and Geim, A.K. (2009) *Rev. Mod. Phys.*, **81**, 109.
13. Frank, I.W., Tanenbaum, D.M., van der Zande, A.M., and McEuen, P.L.J. (2007) *Vac. Sci. Technol.*, **25**, 2558–2561.
14. Boehm, H.P., Clauss, A., Fischer, G., and Hofmann, U. (1962) *Proceedings of the Fifth Conference on Carbon*, Pergamon Press, London, p. 73.
15. Boehm, H.P., Clauss, A., Fischer, G.O., and Hofmann, U. (1962) *Z. Naturforsch.*, **17**, 150.
16. Lerf, A., He, H., Forster, M., and Klinowski, J. (1998) *J. Phys. Chem. B*, **102**, 4477–4482.
17. Szabo, T. *et al.* (2006) *Chem. Mater.*, **18**, 2740–2749.
18. Gao, W., Alemany, L.B., Ci, L., and Ajayan, P.M. (2009) *Nat. Chem.*, **1**, 403.
19. Stankovich, S., Dikin, D.A., Dommett, G.H.B., Kohlhaas, K.M., Zimney, E.J., Stach, E.A., Piner, R.D., Nguyen, S.T., and Ruoff, R.S. (2006) *Nature*, **442**, 282.
20. Stankovich, S., Dikin, D.A., Piner, R.D., Kohlhaas, K.A., Kleinhammes, A., Jia, Y., Wu, Y., Nguyen, S.T., and Ruoff, R.S. (2007) *Carbon*, **45**, 1558.
21. Boukhvalov, D.W. and Katsnelson, M.I. (2008) *J. Am. Chem. Soc.*, **130**, 10697–10701.
22. Song, M. and Cai, D. (2012) in *Polymer–Graphene Nanocomposites*, RSC Nanoscience and Nanotechnology, vol. 26 (ed. V. Mittal), The Royal Society of Chemistry, pp. 1–52.
23. Dreyer, D.R., Murali, S., Zhu, Y., Ruoff, R.S., and Bielawski, C.W. (2011) *J. Mater. Chem.*, **21**, 3443.
24. Fan, X., Peng, W., Li, Y., Li, X., Wang, S., Zhang, G., and Zhang, F. (2008) *Adv. Mater.*, **20**, 4490.
25. Shin, H.J., Kim, K.K., Benayad, A., Yoon, S.M., Park, H.K., Jung, I.S., Jin, M.H., Jeong, H.K., Kim, J.M., Choi, J.Y., and Lee, Y.H. (2009) *Adv. Funct. Mater.*, **19**, 1987.
26. Fernandez-Merino, M.J., Guardia, L., Paredes, J.I., Villar-Rodil, S., Solζs-Fernandez, P., Martζnez-Alonso, A., and Tascon, J.M.D. (2010) *J. Phys. Chem. C*, **114**, 6426.
27. Pei, S., Zhao, J., Du, J., Ren, W., and Cheng, H.M. (2010) *Carbon*, **48**, 4466.
28. Moon, I.K., Lee, J., Ruoff, R.S., and Lee, H. (2010) *Nat. Commun.*, **1**, 73.
29. Chen, W., Yan, L., and Bangal, P.R. (2010) *J. Phys. Chem. C*, **114**, 19885.
30. Liu, S., Tian, J., Wang, L., and Sun, X. (2011) *Carbon*, **49**, 3158.
31. Zhou, X., Zhang, J., Wu, H., Yang, H., Zhang, J., and Guo, S. (2011) *J. Phys. Chem. C*, **115**, 11957.

32. Fan, Z., Wang, K., Wei, T., Yan, J., Song, L., and Shao, B. (2010) *Carbon*, **48**, 1686.
33. Fan, Z., Kai, W., Yan, J., Wei, T., Zhi, L., Feng, J., Ren, Y., Song, L., and Wei, F. (2011) *ACS Nano*, **5**, 191.
34. Chen, D., Li, L., and Guo, L. (2011) *Nanotechnology*, **22**, 325601.
35. Zhou, T., Chen, F., Liu, K., Deng, H., Zhang, Q., Feng, J., and Fu, Q. (2011) *Nanotechnology*, **22**, 045704.
36. Schniepp, H.C., Li, J.L., Mc Allister, M.J., Sai, H., Herrera-Alonso, M., Adamson, D.H., Prud'homme, R.K., Car, R., Saville, D.A., and Aksay, I.A. (2006) *J. Phys. Chem. B*, **110**, 8535.
37. Cote, L.J., Cruz-Silva, R., and Huang, J. (2009) *J. Am. Chem. Soc.*, **131**, 11027.
38. Zhou, M., Wang, Y., Zhai, Y., Zhai, J., Ren, W., Wang, F., and Dong, S. (2009) *Chem. Eur. J.*, **15**, 6116.
39. An, S.J., Zhu, Y., Lee, S.H., Stoller, M.D., Emilsson, T., Park, S., Velamakanni, A., An, J., and Ruoff, R.S. (2010) *J. Phys. Chem. Lett.*, **1**, 1259.
40. Suslick, K.S. (1990) *Science*, **247**, 1439–1445.
41. Hernandez, Y., Nicolosi, V., Lotya, M., Blighe, F.M., Sun, Z.Y., De, S., McGovern, I.T., Holland, B., Byrne, M., Gun'ko, Y.K., Boland, J.J., Niraj, P., Duesberg, G., Krishnamurthy, S., Goodhue, R., Hutchison, J., Scardaci, V., Ferrari, A.C., and Coleman, J.N. (2008) *Nat. Nanotechnol.*, **3**, 563–568.
42. Coleman, J.N. (2013) *Acc. Chem. Res.*, **46**, 14–22.
43. Blake, P., Brimicombe, P.D., Nair, R.R., Booth, T.J., Jiang, D., Schedin, F., Ponomarenko, L.A., Morozov, S.V., Gleeson, H.F., Hill, E.W., Geim, A.K., and Novoselov, K.S. (2008) *Nano Lett.*, **8**, 1704–1708.
44. Bourlinos, A.B., Georgakilas, V., Zboril, R., Steriotis, T.A., and Stubos, A.K. (2009) *Small*, **5**, 1841–1845.
45. Hamilton, C.E., Lomeda, J.R., Sun, Z., Tour, J.M., and Barron, A.R. (2009) *Nano Lett.*, **9**, 3460.
46. Misik, V. and Riesz, P. (1996) *Free Radical Biol. Med.*, **20**, 129.
47. Guittonneau, F., Abdelouas, A., Grambow, B., and Huclier, S. (2010) *Ultrason. Sonochem.*, **17**, 391.
48. Khan, U., O'Neil, A., Loyta, M., De, S., and Coleman, J.N. (2010) *Small*, **6**, 864–871.
49. Dreyer, D.R., Park, S., Bielawski, C.W., and Ruoff, R.S. (2010) *Chem. Soc. Rev.*, **39**, 228–240.
50. Quintana, M., Grzelczak, M., Spyrou, K., Kooi, B., Bals, S., Van Tendeloo, G., Rudolf, P., and Prato, M. (2012) *Chem. Commun.*, **48**, 12159–12161.
51. León, V., Quintana, M., Herrero, M.A., Fierro, J.L.G., de la Hoz, A., Prato, M., and Vázquez, E. (2011) *Chem. Commun.*, **47**, 10936.
52. Cote, L.J., Kim, F., and Huang, J. (2009) *J. Am. Chem. Soc.*, **131**, 1043–1049.
53. Gengler, R.Y.N., Velingura, A., Enotiadis, A., Diamanti, E.K., Gournis, D., Józsa, C., Wees, B.J.V., and Rudolf, P. (2010) *Small*, **6**, 35.
54. Emtsev, K.V., Bostwick, A., Horn, K., Jobst, J., Kellogg, G.L., Ley, L., McChesney, J.L., Ohta, T., Reshanov, S.A., Rotenberg, E., Schmid, A.K., Waldmann, D., Weber, H.B., and Seyller, T. (2009) *Nat. Mater.*, **8**, 203.
55. Sutter, P.W., Flege, J.I., and Sutter, E.A. (2008) *Nat. Mater.*, **7**, 406.
56. Coraux, J., N'Diaye, A.T., Busse, C., and Michely, T. (2008) *Nano Lett.*, **8**, 565.
57. Kim, K.S., Zhao, Y., Jiang, H., Lee, S.Y., Kim, J.M., Kim, K.S., Ahn, J.H., Kim, P., Choi, J.Y., and Hong, B.H. (2009) *Nature*, **457**, 706.
58. Rina, A., Jia, X., Ho, J., Nezich, D., Son, H., Bulovic, V., Dresselhaus, M.S., and Kong, J. (2009) *Nano Lett.*, **9**, 30.
59. Li, X., Cai, W., An, J., Kim, S., Nah, J., Yang, D., Piner, R., Velamakanni, A., Jung, I., Tutuc, E.K., Banerjee, S.K., Colombo, L., and Ruoff, R.S. (2009) *Science*, **324**, 1312.
60. Batzill, M. (2012) *Surf. Sci. Rep.*, **67**, 83–115.
61. Mattevi, C., Kim, H., and Chhowalla, M. (2011) *J. Mater. Chem.*, **21**, 3324.
62. Terrones, M., Botello-Méndez, A.R., Delgado, J.C., López-Urías, F., Vega-Cantú, Y.I., Rodríguez-Macías, F.J., Elías, A.L., Munoz-Sandoval, E., Cano-Márquez, A.G., Charlier, J.C., and Terrones, H. (2010) *Nano Today*, **5**, 351.

63. Han, M.Y., Özyilmaz, B., Zhang, Y., and Kim, P. (2007) *Phys. Rev. Lett.*, **98**, 206805.
64. Jiao, L., Wang, X., Diankov, G., Wang, H., and Dai, H. (2010) *Nat. Nanotechnol.*, **5**, 321.
65. Gomez-Navarro, C., Weitz, R.T., Bittner, A.M., Scolari, M., Mews, A., Burghard, M., and Kern, K. (2007) *Nano Lett.*, **7**, 3499.
66. Tombros, N., Jozsa, C., Popinciuc, M., Jonkman, H.T., and van Wees, B.J. (2007) *Nature*, **448**, 571.
67. Novoselov, K.S. *et al.* (2005) *Proc. Natl. Acad. Sci. U.S.A.*, **102**, 10451.
68. Huang, P.Y., Ruiz-Vargas, C.S., van der Zande, A.M., Whitney, W.S., Levendorf, M.P., Kevek, J.W., Garg, S., Alden, J.S., Hustedt, C.J., Zhu, Y., Park, J., McEuen, P.L., and Muller, D.A. (2011) *Nature*, **469**, 389.
69. Jinschek, J.R., Yucelen, E.H., Calderon, A., and Freitag, B. (2011) *Carbon*, **49**, 556–562.
70. Ferrari, A.C., Meyer, J.C., Scardaci, V., Casiraghi, C., Lazzeri, M., Mauri, F., Piscanec, S., Jiang, D., Novoselov, K.S., Roth, S., and Geim, A.K. (2006) *Phys. Rev. Lett.*, **97**, 187401.
71. Parka, J.S., Reina, A., Saito, R., Kong, J., Dresselhaus, G., and Dresselhaus, M.S. (2009) *Carbon*, **47**, 1303–1310.
72. Tuinstra, F. and Koenig, J. (1970) *J. Chem. Phys.*, **53**, 1126.
73. Mohiuddin, T., Lombardo, A., Nair, R., Bonetti, A., Savini, G., Jalil, R., Bonini, N., Basko, D., Galiotis, C., Marzari, N., Novoselov, K., Geim, A., and Ferrari, A. (2009) *Phys. Rev. B*, **79** (20), 205433.
74. De, S., King, P.J., Lotya, M., O'Neill, A., Doherty, E.M., Hernandez, Y., Duesberg, G.S., and Coleman, J.N. (2009) *Small*, **6**, 1–7.
75. Wang, G., Yang, J., Park, J., Gou, X., Wang, B., Liu, H., and Yao, J. (2008) *J. Phys. Chem. C*, **112**, 8192–8195.
76. Bourlinos, A.B., Georgakilas, V., Zboril, R., Steriotis, T.A., Stubos, A.K., and Trapalis, C. (2009) *Solid State Commun.*, **149**, 2172–2176.
77. Jung, I., Pelton, M., Piner, R., Dikin, D.A., Stankovich, S., Watcharotone, S., Hausner, M., and Ruoff, R.S. (2007) *Nano Lett.*, **7**, 3569.
78. Ni, Z.H., Chen, W., Fan, X.F., Kuo, J.L., Yu, T., Wee, A.T.S., and Shen, Z.X. (2008) *Phys. Rev. B*, **77**, 115416.
79. Blake, P., Hill, E.W., Neto, A.H.C., Novoselov, K.S., Jiang, D., Yang, R., Booth, T.J., and Geim, A.K. (2007) *Appl. Phys. Lett.*, **91**, 063124.
80. Nair, R.R., Blake, P., Grigorenko, A.N., Novoselov, K.S., Booth, T.J., Stauber, T., Peres, N.M.R., and Geim, A.K. (2008) *Science*, **320**, 1308.
81. Sun, Z., Yan, Z., Yao, J., Beitler, E., Zhu, Y., and Tour, J.M. (2010) *Nature*, **468**, 549–552.
82. Lee, D.Y., Khatun, Z., Lee, J.H., and Lee, Y.K. (2011) *Biomacromolecules*, **12**, 336–341.
83. Dong, Y., Chen, C., Zheng, X., Gao, L., Cui, Z., Yang, H., Guo, C., Chi, Y., and Li, C.M. (2012) *J. Mater. Chem.*, **22**, 8764.
84. Pan, D., Zhang, J., Li, Z., and Wu, M. (2010) *Adv. Mater.*, **22**, 734–738.
85. Shen, J., Zhu, Y., Yang, X., Zong, J., Zhang, J., and Li, C. (2012) *New J. Chem.*, **36**, 97–101.
86. Xie, M., Su, Y., Lu, X., Zhang, Y., Yang, Z., and Zang, Y. (2013) *Mater. Lett.*, **93**, 161–164.
87. Yang, F., Zhao, M., Zheng, B., Xiao, D., Wo, L., and Guo, Y. (2012) *J. Mater. Chem.*, **22**, 25471.
88. Zhang, M., Bai, L., Shang, W., Xie, W., Ma, H., Fu, Y., Fang, D., Sun, H., Fan, L., Han, M., Liu, C., and Yang, S. (2012) *J. Mater. Chem.*, **22**, 7461.
89. Wang, F., Zhang, Y., Tian, C., Girit, C., Zettl, A., Crommie, M., and Shen, Y.R. (2008) *Science*, **320**, 206.
90. Zhang, Y., Tang, T.T., Girit, C., Hao, Z., Martin, M.C., Zettl, A., Crommie, M.F., Shen, Y.R., and Wang, F. (2009) *Nature*, **459**, 820.
91. Zhang, H.B., Zheng, W.G., Yan, Q., Yang, Y., Wang, J.W., Lu, Z.H. *et al.* (2010) *Polymer*, **51**, 1191–1196.